INORGANIC CHEMISTRY FRONTIERS

RESEARCH ARTICLE

View Article Online
View Journal

Check for updates

Cite this: DOI: 10.1039/d6qi00716c

Platinum(II)-CN/SCN-rhenium(I) luminophores adopting multiple aggregation states

Viktoria V. Khistiaeva, [a] Victoria Cappellari, [b] Andrey Belyaev, [a] Toni Eskelinen, [c,d] Antti J. Karttunen, [c] Cristian A. Strassert *[b] and Igor O. Koshevoy *[a]

Received 6th April 2026,
Accepted 25th May 2026

DOI: 10.1039/d6qi00716c

rsc.li/frontiers-inorganic

Cycloplatinated complexes constitute an important class of luminescent compounds for sensing, bio-imaging and optoelectronics. Their properties often depend on intermolecular non-covalent interactions between sterically unhindered square planar motifs. Here we investigated the photophysical behavior of novel platinum(II)–rhenium(I) cyanido-/thiocyanato-bridged complexes [{Pt(C^N^N)}(μ-CN/SCN){Re(phen)(CO)$_3$}]$^+$ ($^-$C^N^N = cyclometalated pincer ligand, phen = 1,10-phenanthroline) containing two chromophoric units. Their phosphorescence is dominated in solution by the platinum(II) fragment derived from HC^N^N = phenylbipyridine, while major contribution of the rhenium(I) motif and dual emission are observed when HC^N^N = phenyl-pyrazolylpyridine and triazolyl-phenylpyridine ligand precursors are used. The solid-state behavior depends on intermolecular interactions between platinum components, the preferential mode of which is defined by the counterions. The complexes showcase a rare example of platinum(II)-based bichromophoric compounds demonstrating vapo-/mechano-/thermo-induced reversible changes of optical properties and phase transformations, which could be interpreted as a result of switching between several conformations of noncovalently bound dimers.

Introduction

The versatile photophysical behavior of platinum(II) complexes with π-conjugated organic ligands is often associated with non-covalent π–π and Pt···Pt interactions between molecular fragments.[1,2] Their square-planar geometry favors the formation of ground state assemblies and excimeric species with dramatically lowered absorption and photoluminescence energies resulting in fascinating color phenomena in liquid solutions and in the solid state.[3] The relatively weak metallophilic contacts, which are comparable to hydrogen bonding, are highly sensitive to external triggers that open a way to molecular materials with stimuli-responsive properties such as vapo-, mechano-, thermo-, and solvatochromism.[4–7] In general, the alteration of the photophysical characteristics thus stems from inter- or intramolecular motion that changes the distance between Pt(II)-based chromophores and concomitantly switches the excited state of the system between that of the monomer (conventionally having intraligand excited-state character mixed with metal to ligand charge transfer nature, *i.e.*, M/ILCT), and that of an aggregate exhibiting transitions based on metal–metal-to-ligand charge-transfer states (MMLCT). The illustrative two-state reversible transformations accompanied by contrasting variations of photoemission have been demonstrated for some dinuclear complexes, which exhibit butterfly-type[8,9] or folding/unfolding[10–13] intramolecular conformational changes in solution in response to solvent polarity, acidity, and temperature.

In the solid state, where large intramolecular movements are substantially restricted by a rigid environment, the perturbation of intermolecular contacts plays a dominating role in the optical switching of organometallic platinum(II)-based materials.[6,14] In many cases, bathochromic shifts, induced by mechanical grinding and inverted by fuming with certain organic vapors, occur between crystalline and amorphous phases and are qualitatively attributed to the contraction of metal···metal distances in randomly oriented aggregates.[15–25] The non-covalent interactions within ionic materials increase possible scenarios for stimuli-responsive behavior.[7,26,27] For instance, soft salts composed of Pt(II) chromophore cations and anions form organized nanostructures and display excitation-dependent, aggregation-enhanced, and multistimuli-sensitive luminescence that is associated with variations of

[a]*Department of Chemistry and Sustainable Technology, University of Eastern Finland, P.O. Box 111, FI-80100 Joensuu, Finland. E-mail: igor.koshevoy@uef.fi*
[b]*Institut für Anorganische und Analytische Chemie, CeNTech, SoN, CiMIC, Universität Münster, Heisenbergstraße 11, 48149 Münster, Germany. E-mail: cstra_01@uni-muenster.de*
[c]*Department of Chemistry and Materials Science, Aalto University, FI-00076 Aalto, Finland*
[d]*Institute for Chemical Research, Kyoto University, Uji, Kyoto 611-0011, Japan*

Open Access Article. Published on 01 June 2026. Downloaded on 6/3/2026 5:39:24 AM. This article is licensed under a Creative Commons Attribution 3.0 Unported Licence.

Open Access Article. Published on 01 June 2026. Downloaded on 6/3/2026 5:39:24 AM. This article is licensed under a Creative Commons Attribution 3.0 Unported Licence.

inter-ion interactions and morphological transformations.[28–33] Furthermore, co-crystallized solvents and counterions might yield several interconvertible solvatomorphs and multicolor changes arising from alteration of the geometry of supramolecular stacks.[15,20,34–37] These solvent-triggered phase transitions with contrasting photophysical properties are typically described as relatively small in-plane displacements of parallel Pt(II) molecular constituents.[34] In addition, stimuli-driven rotational movements around the Pt···Pt axis that change the dihedral angle and orientation of the components between antiparallel and staggered conformations also strongly affect the emission energy,[38] pointing out that the metal···metal distance is not the only factor defining optical properties of these materials. Thus, although basic principles of intermolecular dynamics for platinum(II) complexes are understood, the control and details of aggregation states in correlation with distinct optical readout often remain obscure and lack structural proof.

The prevailing majority of platinum(II) complexes showing stimuli-responsive solid-state behavior is represented by mono- and some dinuclear species composed of the same units.[2,5,7,27] Among heterobimetallic Pt(II) compounds such properties were predominantly reported for cluster compounds.[39–41] Responsive Pt(II) compounds constructed of two different photofunctional complex constituents are underexplored in this respect,[27] despite the fact that they could bring new features to excited state behavior by means of intra-/intermolecular charge or energy transfer, formation of new supramolecular arrangements along with multistep transitions between aggregation states.

Pt(II)-containing heterochromophoric species are not exceptional.[42–44] One simple way to assemble bimetallic Pt(II) derivatives relies on the use of pseudohalide cyanido and thiocyanato ligands, which are versatile building blocks due to their ambidentate nature, enabling connection of metal ions into variety of homo- and heterometallic multinuclear architectures including photofunctional aggregates.[45–50] In this view, (CN^-/SCN^-)-decorated Pt(II)-based luminophores[51–55] can serve as metalloligands for the design of multichromophoric species. The feasibility of this approach is supported by the examples of cyanido-bridged compounds comprising cyclometalated Pt(II) moieties. Recently, luminescent cyanido-bridged diplatinum complexes composed of [Pt(C^N)(*p*-MeC_6H_4)] and $[Pt(C^N^N)]^+$ motifs were described by Lalinde/Moreno[56] and our groups.[57]

In this work we synthesized a family of platinum–rhenium complexes, $[\{Pt(C^N^N)\}(\mu\text{-CN/SCN})\{Re(phen)(CO)_3\}]^+$, the first examples of cyanido-/thiocyanato-bridged bichromophoric systems built from cycloplatinated luminophores. The resulting compounds are intensely photoemissive in the solid state (Φ_{em} up to 78%), showing up to an order of magnitude enhancement of the quantum yields compared to the individual constituents. These crystalline materials display reversible mechano-, thermo- and vapochromic changes of photoemission. Notably, the SCN-based derivative shows stimuli-responsive behavior that depends on the counterion and can involve an alteration of intermolecular interactions between platinum fragments resulting in several structurally different aggregation modes.

Results and discussion

Synthesis and structural characterization

The reaction of neutral cyanido precursors such as [Pt(C^N^N)(CN)][58] (derived from HC^N^N = 6-phenyl-2,2′-bipyridine Hphbpy, 2-phenyl-6-(1*H*-pyrazol-1-yl)pyridine Hphpypz, or 2-(1-benzyl-1*H*-1,2,3-triazol-4-yl)-6-phenylpyridine Hphpytabn) with a labile derivative of rhenium(I) tricarbonyl [Re(phen)$(CO)_3(H_2O)$][$BAr^F{}_4$] (phen = 1,10-phenanthroline; $^-BAr^F{}_4$ = tetrakis[3,5-bis(trifuoromethyl)phenyl]borate) carried out for two days afforded heterobimetallic compounds [{Pt(C^N^N)}(CN){Re(phen)}][$BAr^F{}_4$] (**1–3**), which were isolated as stable greenish to orange crystalline materials in good yields (85–88%, Scheme 1A; see the SI for experimental details).

The bulky fluorinated counterion $^-BAr^F{}_4$ was used for improved solubility.

An alternative approach was used for the preparation of the thiocyanato-bridged derivative [{Pt(phbpy)}(SCN){Re(phen)}][CF_3SO_3] starting from the [Re(phen)$(CO)_3$(NCS)] and [Pt(phbipy)(NCMe)][CF_3SO_3] complexes (**4a**, Scheme 1B). The triflate salt **4a** was obtained as bright red powder, the subsequent anion metathesis for $^-BAr^F{}_4$ afforded **4** as a yellow solid.

Mass-spectrometry performed in the ESI^+ mode confirmed the assembly of the bimetallic compounds and revealed the major signals corresponding to molecular ions (Fig. S1). The ^1H NMR spectra of **1–4** recorded in CD_2Cl_2 show the patterns comprising characteristic resonances of the {Re(phen)} and {Pt(C^N^N)} fragments in a 1 : 1 ratio (Fig. S2–S6). The obvious differences in chemical shifts observed for **4a** and **4** having the same cation and at comparable concentrations (Fig. S5 and S6) probably arise from alteration of anions due to ion pairing effects occurring in moderately polar dichloromethane.

The solid-state IR spectra of these complexes display strong CO stretching vibrations around 2027–2037 and 1940–1910 cm^{-1}, which are typical frequencies for rhenium *fac*-tricarbonyl derivatives.[46,59–61] The moderately strong signals at 2146–2156 cm^{-1} are assigned to the ν(CN)mode of the cyanide and thiocyanate bridges.[51,62]

All title compounds **1–4** and **4a** were investigated crystallographically. Notably, **4** and **4a** are the first ever structurally characterized Pt–Re thiocyanato-bridged complexes. Their molecular views are depicted in Fig. 1, 2 and S7 (ESI); Table S1 lists crystal and refinement data. In line with spectroscopic results, molecular cations of **1–4** consist of {Re(phen)$(CO)_3$} and {Pt(C^N^N)} units connected by the μ-C,N or μ-S,N ligands. The metal ions adopt pseudo-octahedral (Re) and quasi-square planar (Pt) geometries with structural characteristics (Tables S2 and S3) resembling those of their mononuclear relatives [Pt(C^N^N)(CN)],[53,58] [Pt(N^C^N)(SCN)][54] and [Re(phen)$(CO)_3$X].[46,60,61] The CN^- bridge is likely coordinated

This journal is © the Partner Organisations 2026

Open Access Article. Published on 01 June 2026. Downloaded on 6/3/2026 5:39:24 AM.
This article is licensed under a Creative Commons Attribution 3.0 Unported Licence.

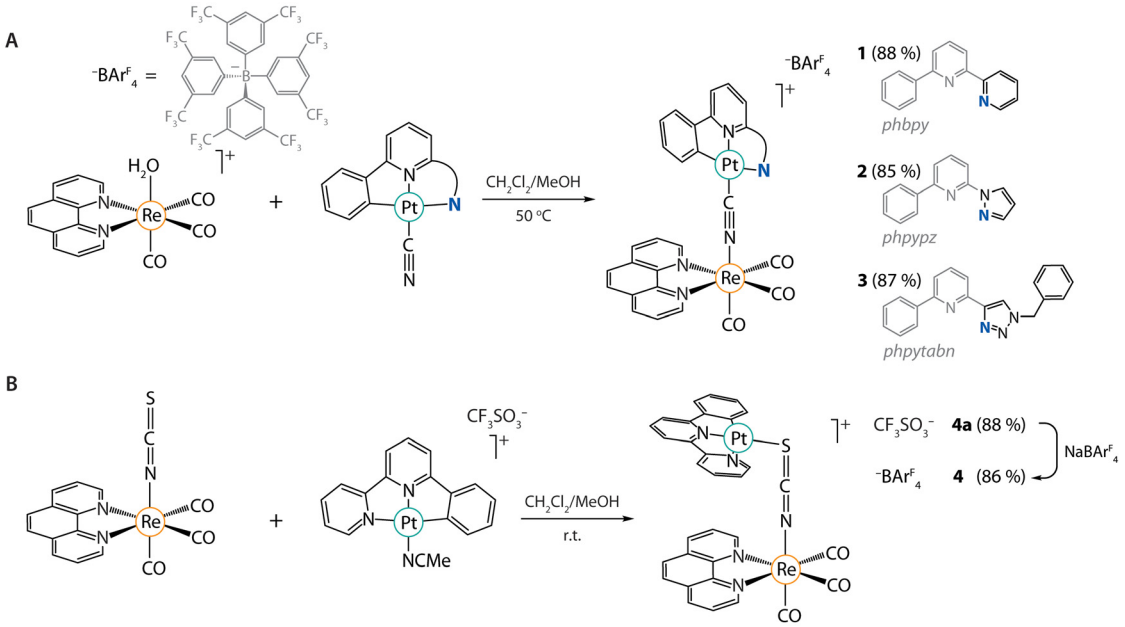

Scheme 1 Syntheses of complexes **1–3** (A) and **4a**, **4** (B).

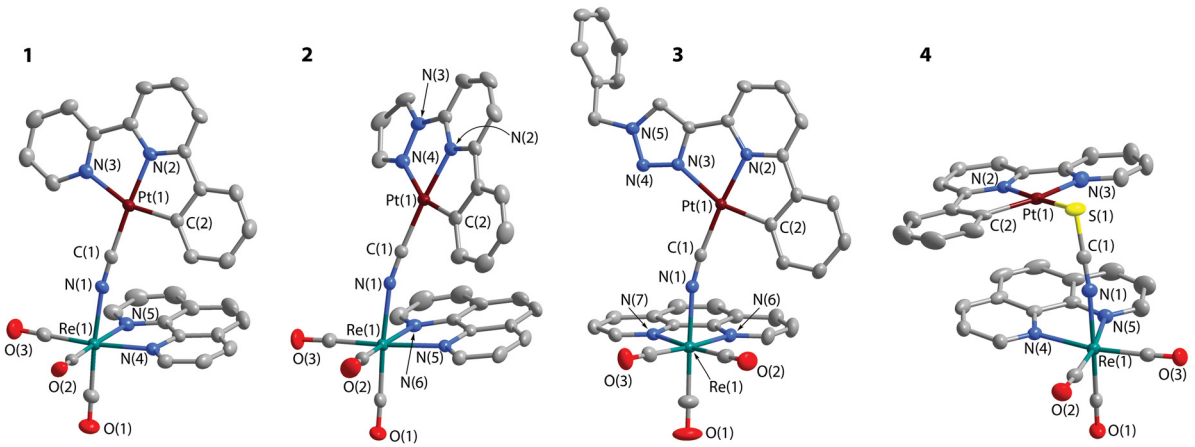

Fig. 1 Molecular views of the salts **1–4** (displacement ellipsoids are at 50% probability level; hydrogen atoms, crystallization solvents and $^{-}BAr^{F}_{4}$ counterions are omitted for clarity).

to the rhenium and platinum centres *via* N and C atoms, respectively, reflecting a higher affinity of Pt(II) to the carbanionic donor. The thiocyanato linker in **4** and **4a** is found in a Pt–SCN–Re mode, while both S- and N-linkage isomers are known in the case of terminal bonding to platinum(II).[54,63] The ∠Pt–S–C angle of 95.49(7)° in **4** leads to a tweezer-like molecular shape with the shortest interatomic distances between phen and phbpy ligands being in the range of 3.33–3.45 Å.

This configuration resembles that observed for bimetallic Pt–Ir complexes with intramolecular stacking between phenylpyridine/phenylisoquinoline and terpyridine ligands bound to Ir and Pt ions, respectively.[43]

Crystal packing of **1–4** reveals intermolecular π–π stacking between cycloplatinated components having a head-to-tail orientation that causes formation of dimers in the solid state (Fig. S7). The Pt···Pt distances in **1**, **3** and **4** exceed 3.6 Å, thus implying a lack of metallophilic interactions. In **2**, the metal–metal separation is 3.2584(7) Å, tilted with respect to the plane of the phpypz ligand, ∠Pt–Pt–N(2) = 80.45(7)°. Despite the fact that this Pt···Pt contact is shorter than the sum of van der Waals radii, the yellow color of crystals of **2** suggests inefficiency of intermolecular bonding as low energy charge-transfer states do not become accessible in the ground state (see the discussion of the photophysical properties below).

Unlike the $^{-}BAr^{F}_{4}$ salt **4**, its triflate analog **4a** was found in several forms: a minor yellow metastable **4a_y**(CH_2Cl_2) and the main red **4a_r**(CH_2Cl_2) dichloromethane modifications, the red acetone solvate **4a_r**(acetone), and a very minor solvent-free

Open Access Article. Published on 01 June 2026. Downloaded on 6/3/2026 5:39:24 AM. This article is licensed under a Creative Commons Attribution 3.0 Unported Licence.

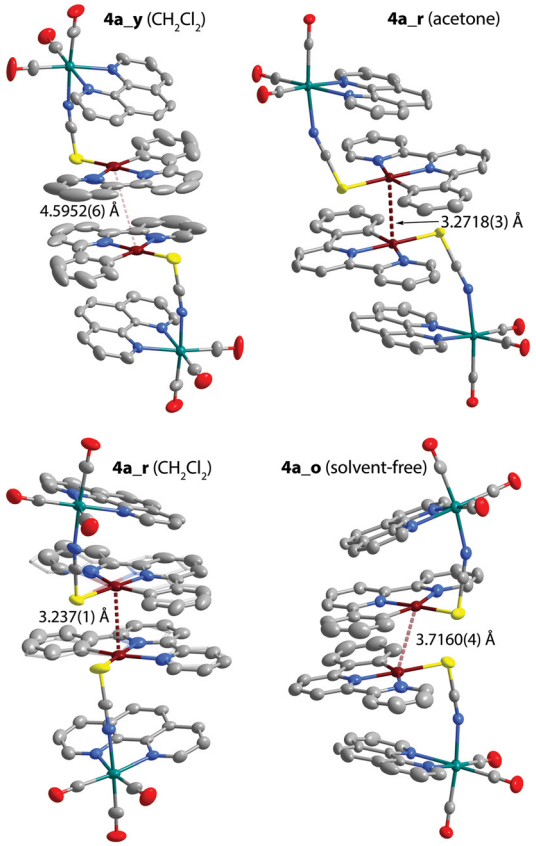

Fig. 2 Dimers of cations in modifications of triflate salt **4a_y**(CH_2Cl_2), **4a_r**(acetone), **4a_r**(CH_2Cl_2), and **4a_o** (the distances correspond to Pt···Pt separations; the minor component of the disorder in **4a_r** (CH_2Cl_2) is shown in semi-transparent stick mode; displacement ellipsoids are at 50% probability level; hydrogen atoms, crystallization solvents and $CF_3SO_3^-$ counterions are omitted for clarity).

orange polymorph **4a_o**, which appeared along with **4a_r** (acetone) from dilute solution at the late stage of crystallization. These species have the same composition and stereochemistry of the bimetallic cation [{Pt(phbpy)}(SCN){Re(phen)}]$^+$, but show different mutual orientation in dimeric species (Fig. 2). The intermolecular arrangement of **4a_y**(CH_2Cl_2) is similar to that of **4** with{Pt(phbpy)} fragments forming a head-to-tail stack with long Pt···Pt separation (4.5952(6) Å). In the major deep red dichloromethane solvate **4a_r**(CH_2Cl_2), the cycloplatinated moieties are placed in a rather rare head-to-head manner[57] with metal–metal distance shortened to 3.237(1) Å, although an accurate evaluation of this bond length is hampered by the disorder, which involves one platinum centre. Cocrystallization with acetone induces more conventional head-to-tail disposition of stacked {Pt(phbpy)} motifs in red **4a_r**(acetone) also having a short platinum–platinum contact of 3.2718(3) Å. Minor form **4a_o** somewhat resembles **4a_r**(CH_2Cl_2) but has a longer intermolecular Pt···Pt separation of 3.7160(4) Å and a larger dihedral angle S–Pt–Pt–S (53.9 *vs.* 27.7°). Further details of **4a** are discussed below in relation to the solid-state photoluminescence behavior.

Photophysical properties in solution and theoretical analysis

The electronic absorption spectra of compounds **1–4** and **4a** in dichloromethane solutions under ambient conditions are shown in Fig. 3 and the data are listed in Table 1. The spectroscopic patterns represent superpositions of the spectra generated by individual metal-containing components. Intense absorption bands at wavelengths below *ca.* 320 nm correspond to transitions into intraligand states (IL, *i.e.*, π–π* configurations) in phen and C^N^N ligands, as reported for [Re(phen)$(CO)_3$L]^x (ref. 60, 64 and 65) and [Pt(C^N^N)L]^x (ref. 57) compounds, as well as some mixed Re–Pt species.[66] The lower energy region around 350 nm with tails extending above 450 nm is dominated by structured bands of moderate intensities ($\varepsilon \sim 1.5 \times 10^4$ M^{-1} cm^{-1}), which are consistent with those of [{Pt(C^N^N)}$_2$CN]$^+$ complexes with analogous ligands,[57] and therefore are attributed to transitions into states with an admixture of metal-to-ligand and intraligand charge transfer (^{1}ML/^{1}ILCT) character occurring within the {Pt(C^N^N)} chromophores. These signals evidently overlap with lower intensity bands of the {$Re(CO)_3$} → phen (^{1}MLCT/^{1}LL′CT) origin.[60,64,65] The absence of new bathochromically shifted absorptions implies that no significant intramolecular charge-transfer between the metal constituents takes place. Time-Dependent Density Functional Theory (TD-DFT) computational analysis confirms that the two lowest singlet excited states localized on the platinum(II)- and rhenium(I)-based moieties are energetically very close and both could be populated under the experimental conditions (Fig. 4 and S8, Table S4).

It should be noted that the theoretically assessed excitation and emission energies are substantially method-dependent, as exemplified by complexes **2** and **3** (see the data in Tables S4 and S5), meaning that the prediction of the nature of the lowest excited state could be ambiguous in the view of virtual energetic degeneracy of {Pt} and {Re} centered triplet states.

Complexes **1–4** exhibit moderately intense luminescence in liquid CH_2Cl_2 solutions at room temperature. The sensitivity of the quantum yields to the presence of dissolved triplet dioxygen along with lifetimes in the microsecond regime suggest phosphorescence, which is in line with the data for comparable platinum(II)- and rhenium(I)-derived species.[57,60,65] The unresolved emission profiles of **1** (λ_{em} = 544 nm) and **4**/**4a** (λ_{em} = 560/558 nm) containing {Pt(phbpy)} fragments (Fig. 3) are very close to those of the homometallic relatives [Pt(phbpy)CN] (λ_{em} = 562 nm)[67] and [{Pt(phbpy)}$_2$CN]$^+$ (λ_{em} = 546 nm)[57] pointing to negligible participation of the {Re(phen)$(CO)_3$} chromophore on the radiative excited state T_1, which is consistently reproduced by theoretical analysis (Fig. 4). The quantum yield of **1** (Φ_{em} = 0.22) is twice as high as that of [Pt(phbpy)CN] (Φ_{em} = 0.1) and is close to that of [{Pt(phbpy)}$_2$CN]$^+$ (Φ_{em} = 0.25). However, both these reference complexes show radiative rates k_r of 4.5 and 7.5 × 10^4 s^{-1}, respectively, which are higher than the $k_r = 3.6 \times 10^4$ s^{-1} estimated for **1**. Consequently, the slower radiationless relaxation of the excited state and thus visibly longer lifetime of **1** might be attributed to enhanced rigidity or increased ligand-field splitting, if compared with coordination compounds deco-

This journal is © the Partner Organisations 2026

Open Access Article. Published on 01 June 2026. Downloaded on 6/3/2026 5:39:24 AM.
This article is licensed under a Creative Commons Attribution 3.0 Unported Licence.

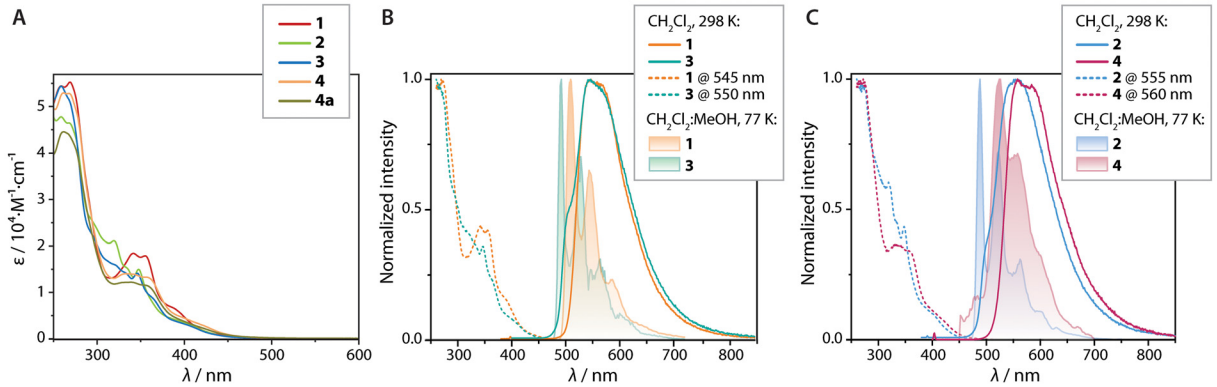

Fig. 3 (A) UV-vis absorption spectra of complexes **1–4**, **4a** (CH_2Cl_2, 298 K); normalized photoluminescence excitation and emission spectra of **1**, **3** (B) and **2**, **4** (C) at 298 K (CH_2Cl_2, $c \approx 5 \times 10^{-6}$ M) and 77 K (CH_2Cl_2 : MeOH, $c \approx 10^{-6}$ M).

Table 1 Photophysical properties of complexes **1–4** and **4a** in liquid solution (CH_2Cl_2, 298 K)

	λ_{abs},[a] nm (ε, 10^4 M^{-1} cm^{-1})	λ_{em},[b] nm	τ_{amp_av} (Ar),[c,d] μs	Φ_{em} (air/Ar)		k_r,[e] 10^4 s^{-1}	k_{nr},[e] 10^4 s^{-1}
1	269 (5.5), 342 (1.8), 355 (1.8), 390sh (0.6)	544 (509)[d]	6.11 ± 0.01 (12.60 ± 0.02)[f]	0.04 ± 0.02	0.22 ± 0.02	3.6 ± 0.3	12.8 ± 0.3
2	259 (4.7), 268 (4.6), 319 (2.1), 348 (1.5), 400sh (0.4)	554 (488)	2.91 ± 0.01 (19.18 ± 0.04)	0.11 ± 0.02	0.33 ± 0.03	11.3 ± 1.0	23.0 ± 1.1
3	259 (5.4), 346 (1.4), 364sh (0.9), 405sh (0.3)	542 (492)	3.26 ± 0.01 (17.25 ± 0.02)	0.08 ± 0.02	0.34 ± 0.03	10.4 ± 0.9	20.2 ± 1.0
4	261 (5.3), 268 (5.3), 332 (1.4), 355 (1.3), 420sh (0.3)	560 (526)	1.11 ± 0.01 (9.01 ± 0.03)	0.03 ± 0.02	0.06 ± 0.02	5.4 ± 1.8	84.7 ± 2.9
4a	262 (4.5), 339 (1.2), 357sh (1.1)	558 (524)	1.09 ± 0.01 (8.44 ± 0.03)	0.03 ± 0.02	0.05 ± 0.02	4.6 ± 1.7	87.2 ± 2.6

[a] CH_2Cl_2. [b] λ_{exc} = 350 nm for **1–3** and 360 nm for **4**, **4a**. [c] Amplitude-weighted average lifetime determined by the equation $\tau_{av} = \sum A_i\tau_i$, A_i = weight of the i-th component. [d] Photoluminescence decays are shown in Fig. S20–S40. [e] Average radiative and nonradiative rate constants under Ar at RT were estimated as follows: $k_r = \Phi_{em}/\tau$, $k_{nr} = (1 - \Phi_{em})/\tau$. [f] Values in parentheses correspond to CH_2Cl_2 : MeOH 1 : 1 frozen glassy matrices at 77 K.

rated with organic chromophores.[68,69] In the case of **4**/**4a**, the effect of {Pt} ↔ {Re} interaction seems to be minimized presumably due to the very fast transfer rate as their k_r values are almost the same as for [Pt(phbpy)CN]. In contrast to **1**, **4**/**4a** are susceptible to more efficient nonradiative deactivation, which accounts for lower quantum yields (Table 1).

The structureless emission bands of compounds **2** and **3** peaking at 554 and 542 nm in CH_2Cl_2 are accompanied by discernible high-energy shoulders around 500 nm (Fig. 3). These minor signals can be tentatively attributed to residual luminescence of {Pt(C^N^N)} units by comparing with the spectra of the corresponding diplatinum cations $[\{Pt(C^N^N)\}_2CN]^+$,[57] which show vibronic progressions maximized at 499 and 503 nm. Hence, the main contribution to the observed phosphorescence of **2** and **3** therefore is made by the {Re(phen)(CO)$_3$} centers. For instance, the multichromophore complexes $[\{Re(phen)(CO)_3\}_xM(CN)_x]^{x/2+}$ emit at 543 (M = Au) and 549 (M = Pt) nm with *ca.* twice faster radiative rates suggesting that {Pt} ↔ {Re} energy transfer is also possible for **2** and **3**.[46]

The DFT calculations (LRC-wPBEh functional) seem to underestimate the energy of the {Pt(C^N^N)} chromophores, which constitute the T_1 state in **2** and **3** (Fig. S8). The PBE0 method, however, localizes the lowest triplet state on the {Re(phen)(CO)$_3$} fragment (Table S5). This points to a small energy gap between the T_1 and T_2 states assigned to different metal components (Table S4) and the sensitivity of the {Re(phen)(CO)$_3$}-MLCT state to the environment. The latter is confirmed by the emission spectra of **2** and **3** showing positive solvatochromism of the charge transfer band in the solvents of higher polarity such as methanol and acetonitrile (Fig. S9). The solvent-independent emission profiles for **1** (Fig. S9) are in line with aforementioned assignment of the T_1 state to the {Pt(phbpy)} fragment.

The luminescence spectra of all complexes **1–4** in diluted CH_2Cl_2:MeOH frozen glassy matrices at 77 K reveal structured blue-shifted signals (Fig. 3 and Table 1), which can be assigned to the {Pt(C^N^N)}-localized transitions attributed mainly to the IL nature of the excited states. This correlates well with the characteristics of $[\{Pt(C^N^N)\}_2CN]^+$ compounds at 77 K (ref. 57) and a pronounced increase of emission energies reported for $[Re(phen)(CO)_3L]^x$ complexes at low temperature in frozen glasses[46,65] that is anticipated to make platinum

Open Access Article. Published on 01 June 2026. Downloaded on 6/3/2026 5:39:24 AM.
This article is licensed under a Creative Commons Attribution 3.0 Unported Licence.

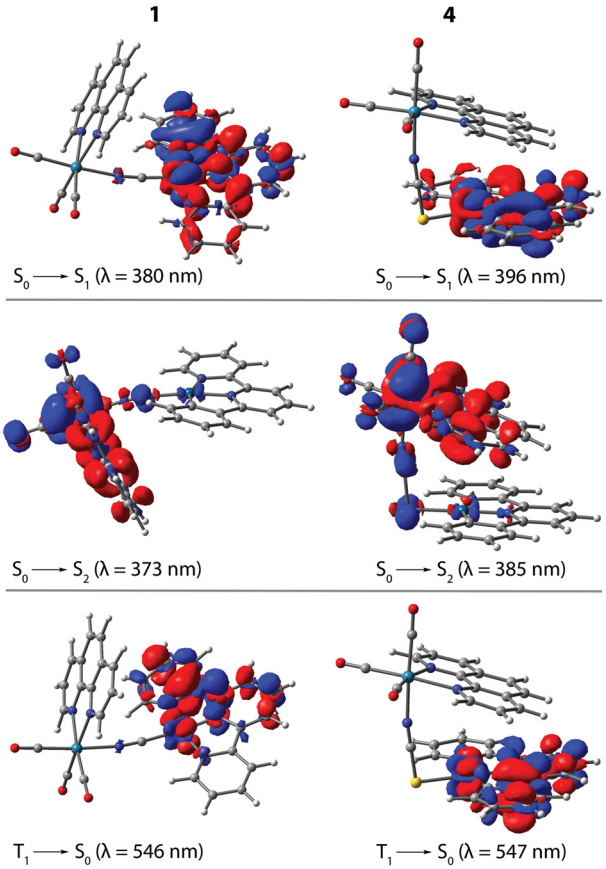

Fig. 4 Selected electron density difference plots for complexes **1** and **4** (LRC-wPBEh in vacuum, isovalue 0.001 a.u.). Along the indicated electronic transition, the electron density mainly decreases in the blue areas and increases in the red areas.

fragments the main contributors to the T_1 states of the title bimetallic compounds.

No long wavelength band was observed around 700 nm for **1–4** at low concentrations of *ca.* 1×10^{-6} M meaning that these complexes are less prone to intermolecular aggregation *via* Pt⋯Pt interaction as homometallic relatives [{Pt(C^N^N)}$_2$CN]$^+$.[57] At room temperature, low energy emission bands (*ca.* 725 nm) emerge for **4** and particularly for **4a** at higher concentrations (7×10^{-4} M, Fig. S10) in dichloromethane and acetone but not in higher polarity acetonitrile and methanol, which enhance the ground state aggregation.[57,70] These observations and the similarity of excitation spectra for high and low energy bands testify in favor of excimers mainly responsible for the near-IR emissions. The higher intensity of the red band for **4a** than for **4** proves that the bulky counterion constrains the formation of excimers.

The assembly of **4a** and **4** was tested in mixtures of solvents using acetone and water (Fig. S11). Triflate complex **4a** shows a gradual growth of the emission band around 730 nm upon the increase of water content indicative of the MMLCT excited state.[21,31,71] Compound **4** with hydrophobic $^-$BAr$^F{}_4$ anion nearly completely aggregates once reaching critical water concentration to give opaque red-emissive systems, which are unstable and ultimately produce microcrystalline precipitates with yellow luminescence.

Photophysical properties in the solid state

The luminescence of solid samples **1–4** and **4a** substantially depends on intermolecular interactions involving cycloplatinated motifs and thus covers a broad range of wavelengths (Table 2 and Fig. 5). The minor forms **4a_y**(CH_2Cl_2) and **4a_o** demonstrate eye-perceived bright yellow and moderate orange luminescence, respectively, but their properties were not investigated as only a few crystals for XRD analysis were isolated. The structureless orange-red emission of **1** peaks at 620 nm falls in between the signals of mononuclear cyanido complexes [Re(phen)(CO)$_3$CN] (λ_{em} = 534 nm, Φ_{em} = 0.04)[60] and [Pt(phbpy)CN] (λ_{em} = 701 nm, Φ_{em} = 0.12).[67] It is likely associated with π–π-stacked platinum fragments lacking metal–metal bonding but possibly perturbed by C–H$_{phen}$⋯π$_{phbpy}$ intermolecular interactions (Fig. S7). Notably, the quantum yield of **1** reaches 0.72 at room temperature, which significantly outperforms those of individual components and is the highest value among the reported [Pt(phbpy)X] derivatives in the solid state. As the radiative rates of **1** and [Pt(phbpy)CN] are close (k_r = 3.85 and 4.0×10^5 s^{-1}, respectively), the gain in efficiency is achieved by suppressing nonradiative relaxation pathways.

Table 2 Photophysical properties of complexes **1–4** and **4a** in the solid state (298 K, air-free conditions)

	λ_{exc}, nm	λ_{em}, nm	τ_{amp_av},[a,b] μs	Φ_{em}	k_r,[c] 10^5 s^{-1}	k_{nr},[c] 10^5 s^{-1}
1	483	620	1.87 ± 0.01	0.72 ± 0.07	3.85 ± 0.04	1.50 ± 0.04
Ground	480	626	1.74 ± 0.01	0.39 ± 0.04	2.24 ± 0.02	3.51 ± 0.03
2	379	562	2.91 ± 0.01	0.78 ± 0.08	2.68 ± 0.03	0.76 ± 0.03
Ground	380	607	2.27 ± 0.01	0.55 ± 0.05	2.42 ± 0.02	1.98 ± 0.03
3	409	526	1.88 ± 0.02	0.10 ± 0.02	0.53 ± 0.01	4.79 ± 0.02
Ground	464	618	2.45 ± 0.01	0.47 ± 0.05	1.92 ± 0.02	2.16 ± 0.02
4	374	570	3.48 ± 0.01	0.20 ± 0.02	0.57 ± 0.01	2.30 ± 0.01
Ground	410	701	0.80 ± 0.02	0.13 ± 0.02	0.61 ± 0.03	3.78 ± 0.06
4a_r(CH_2Cl_2)	527	688	1.08 ± 0.01	0.25 ± 0.02	2.31 ± 0.02	6.94 ± 0.03
Ground	518	702	0.48 ± 0.01	0.12 ± 0.02	2.50 ± 0.05	18.3 ± 0.09
4a_r(acetone)	504	665	1.72 ± 0.01	0.29 ± 0.03	1.69 ± 0.02	4.13 ± 0.02

[a] Amplitude-weighted average lifetime determined by the equation $\tau_{amp\_av} = \sum A_i\tau_i$, A_i = weight of the i-th component. [b] Photoluminescence decays are shown in Fig. S27–S37. [c] Average radiative and nonradiative rate constants were estimated as follows: $k_r = \Phi_{em}/\tau$, $k_{nr} = (1 - \Phi_{em})/\tau$.

This journal is © the Partner Organisations 2026

Open Access Article. Published on 01 June 2026. Downloaded on 6/3/2026 5:39:24 AM.
This article is licensed under a Creative Commons Attribution 3.0 Unported Licence.

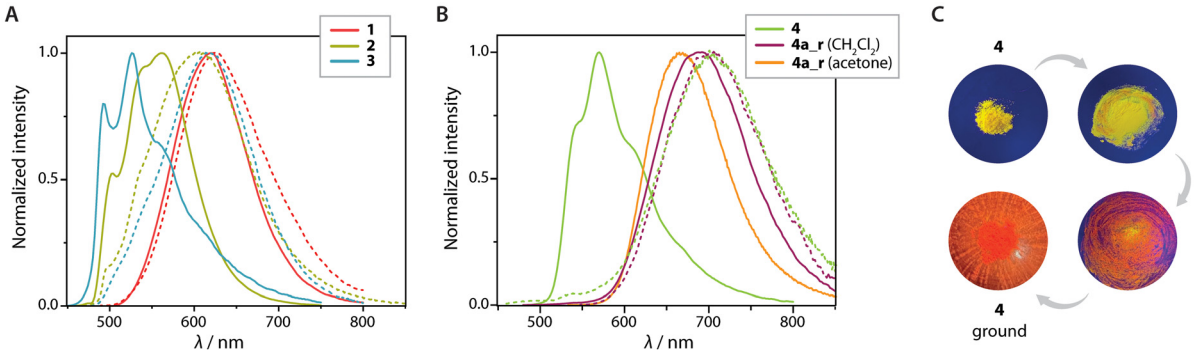

Fig. 5 Normalized photoluminescence emission spectra of dried crystalline (solid lines) and ground (dashed lines) samples of **1–3** (A) and **4**, **4a_r** (B) at 298 K; (C) shows gradual changes of solid-state emission of **4** upon grinding.

Grinding crystalline **1** produces mostly an amorphous phase evidenced by PXRD data (Fig. S12) but has a minor effect on the emission profile while only slightly shifting the maximum by 155 cm^{-1} to 626 nm. On the other hand, disruption of crystal packing visibly decreases the Φ_{em} to 0.39 and k_r to 2.24 × 10^5 s^{-1} that connotes a prominent influence of intermolecular interactions on the deactivation of the excited state.

Dried crystalline samples of **2–4** demonstrate structured emission spectra with maxima at 562, 526 and 570 nm, respectively (Fig. 5). Complex **2** with a high quantum yield of 0.78 is the brightest luminophore in the presented series. The wavelengths correlate with the data recorded for solutions (Table 1), and together with distinguishable vibrational progressions evidence the domination of IL/MLCT excited state character that is confirmed computationally for dimeric species (Table S5 and Fig. S15). Despite a relatively short Pt···Pt separation of 3.2584(7) Å found in complex **2** (Fig. S7), the low-energy metal-to-metal charge transfer (MMLCT) state does not operate in its neat material.

Unlike **1**, the luminescence of compounds **2–4** shows a distinct mechanochromic response. For these complexes, grinding mostly eliminates fine structures of the emission bands and changes the peak wavelengths to 607 (**2**), 618 (**3**) and 701 (**4**) nm that results in a contrasting 3280 cm^{-1} (131 nm) red shift demonstrated by **4**. The reduction of the emission energy in platinum(II) cyclometalated complexes upon grinding is not exceptional and occurs due to shortening of π–π stacking and/or metal···metal contacts.[15,18,35,72–74] The perturbation of stacking interactions leading to excimer-like luminescence in amorphous phases is a probable scenario for **2** and **3**. Thorough grinding of these materials visibly decreases the intensity of their PXRD patterns but nevertheless shows a significant retention of initial crystallinity, particularly in the case of compound **3** (Fig. S13). This observation points to a metastable character of amorphous phases of **2** and **3**, which are nevertheless formed in quantities sufficient for nearly complete excitation energy transfer leading to bathrochromically shifted luminescence. The instability of the ground phases may be caused by restricted formation of metallophilic bonds in **1–3** due to intermolecular {Pt(C^N^N)} ↔ CO steric repulsion in dimeric species (Fig. S7). The weaker Pt···Pt interactions therefore do not allow attaining longer wavelength luminescence (λ_{em} ≥ 700 nm) as shown by their homoplatinum relatives.[57]

On the other hand, the SCN-bridged complex **4** having a bent configuration can be more completely converted into the deep-red amorphous state (Fig. S13), which exhibits a broad low-energy band maximized at 701 nm. This emission likely appears from short Pt···Pt contact and probably eclipsed head-to-head arrangement, *i.e.* the dimer configuration resembling that found in solvate **4a_r**(CH_2Cl_2) of the triflate analog (Fig. 2), which emits at 688 nm (Table 2).

The original green-yellow emissions of crystalline **2–4** can be restored by exposing ground samples to vapors of organic solvents (alcohols, diethyl ether). Similarly, heating amorphous phases of **2–4** at *ca.* 380 K also recovers microcrystalline materials (Fig. S12 and S13) and their intrinsic photophysical characteristics (Fig. S16). Differential scanning calorimetry (DSC, Fig. S17) performed for ground samples of **2–4** revealed exothermic peaks in the range 369–378 K (96–105 °C), which are absent for pristine crystalline compounds. This suggests that metastable amorphous **2–4** undergo thermally induced crystallization. While distinct and reversible shifts of the emission upon mechano-vapor treatment are known for platinum(II) compounds,[18,23,24,74] thermal recovery remains a rather rare phenomenon among Pt(II) phosphors.[16,25,73,75] The phase transition occurs without appreciable decomposition, as compounds are stable to *ca.* 520 K (250 °C, Fig. S18). Such behavior of **2–4** probably originates from the relatively soft nature of materials containing bulky hydrophobic $^{-}BAr^{F}{}_{4}$ anions, which allow the phase transition to occur at moderate temperatures. In line with this hypothesis, the exothermic peak in the DSC thermogram of ground triflate salt **4a** is shifted to 426 K (153 °C) reflecting a denser and less mobile intermolecular packing.

To sum up possible changes in intermolecular interactions, which take place during the interconversions of modifications of **4** and **4a**, the crystallographically characterized forms of the triflate **4a** (Fig. 2) might be used for the illustration schematically depicted in Fig. 6. Thus, the yellow luminescence of crys-

Open Access Article. Published on 01 June 2026. Downloaded on 6/3/2026 5:39:24 AM.
This article is licensed under a Creative Commons Attribution 3.0 Unported Licence.

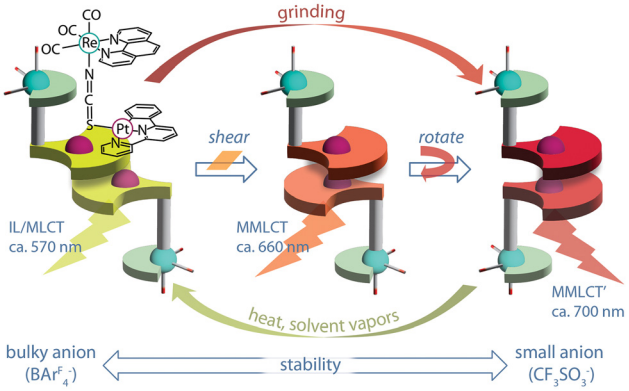

Fig. 6 Schematic summary of structural variations of the dimer of the cation of **4** driven by external stimuli and the anion.

talline **4** aligns well with the visual appearance of a metastable minor yellow form **4a_y**(CH_2Cl_2). Both these compounds have essentially the same arrangement of their dimers with long Pt···Pt separations (Fig. S7 and 2) that result in the phosphorescence from the monomeric {Pt(phbpy)} fragment according to DFT calculations (Table S5 and Fig. S20). The red-emitting modification **4a_r**(acetone) (λ_{em} = 665 nm and Φ_{em} = 0.29) consists of dimeric species, which can be seen as a result of a shear movement of the head-to-tail placed cycloplatinated units in **4**/**4a_y** (Fig. 2). This molecular displacement leads to the formation of intermolecular metallophilic bonding and activates the first low-energy MMLCT excited state. Further decrease in the emission energy is achieved in the red solvate **4a_r**(CH_2Cl_2) (λ_{em} = 688 nm and Φ_{em} = 0.25) featuring head-to-head orientation of the platinum(II) chromophores. The configuration formally corresponds to *ca.* 180° rotation of one molecular component of **4a_r**(acetone) around the axis of the Pt···Pt bond. The possibility of such rotational movement is indicated by the phase changes occurring upon drying sample **4a_r**(acetone), Fig. S19. Prolonged storage of crystalline red **4a_r**(acetone) under ambient conditions (>1 week) or vacuuming at 60 °C for 12 h yields orange material, the PXRD pattern of which matches well the one simulated for solvent-free polymorph **4a_o** (Fig. S14). Despite the phase transformation of **4a_r**(acetone) is not selective and likely gives a mixture of aggregates according to the excitation and emission spectra comprising several bands (Fig. S19), the **4a_o** form seems to be the dominating crystalline component. This process also resembles *ca.* 50° rotation of diplatinum molecules in microrods taking place during the loss of crystallization solvent.[38]

The red shift for **4a_r**(CH_2Cl_2) was adequately described by theoretical analysis, which anticipates the MMLCT-originated phosphorescence at 721 nm (Table S5 and Fig. S20). The head-to-head stack of pincer {Pt(C^N^N)} blocks was earlier predicted to have a narrower optical band gap than more conventional head-to-tail modes.[57] This proves the importance of the angular parameter that defines the orientation of chromophores in the stack but not only of the metal–metal distance. Grinding the triflate **4a_r** solvates produces essentially the same materials showing broad emission in the red region with the maximum around 700 nm (Table 2 and Fig. 5), which is close to that of crystalline **4a_r**(CH_2Cl_2) and could suggest the formation of head-to-head dimers in these materials. The luminescence of ground **4** (λ_{em} = 701 nm) also virtually coincides with that of amorphous **4a_r** and thus can be tentatively explained in terms of a similar head-to-head intermolecular stack (Fig. 6).

This effect of counteranions on the intermolecular association, *i.e.* $^{-}$BAr$^{F}_{4}$ *vs.* triflate in **4** and **4a**, is reminiscent of that of solvent polarity, the increase of which can dramatically promote the formation of the aggregates with close Pt···Pt contacts.[57,70] In addition to possible electronic effects, noted previously for terpyridine-alkynyl compounds,[76] no less important could be the size of anion as has been recently shown for the series of their phosphonium-decorated congeners.[77] The essential outcome from comparison of **4** and **4a** is that with the help of the counterion it might be possible to control the stability of a given aggregation state and to adjust the transitions between several metastable forms.

Conclusions

A series of heterometallic complexes composed of cyclometalated {Pt(C^N^N)} and {Re(phen)(CO)$_3$} chromophores were prepared by using the cyanido (**1–3**) and thiocyanato (**4**, **4a**) bridges. All compounds demonstrate luminescence in solution that depends on the Pt(II)-coordinated pincer ligand and originates mainly from the platinum(II)-based unit (for HC^N^N = phenylbipyridine, **1** and **4**) or the rhenium(I) fragment (for HC^N^N = phenyl-pyrazolylpyridine, triazolyl-phenylpyridine, **2** and **3**). Dual emissions observed for **2** and **3** and longer intrinsic lifetimes *vs.* their monometallic congeners suggest {Pt} ↔ {Re} coupling between energetically close triplet states localized on separate metal components, in line with the results of TD-DFT calculations. In frozen glassy matrices at 77 K, complexes **1–4** emit exclusively from {Pt(C^N^N)}-centered excited states with ^{3}(ML/ILCT) configuration apparently due to destabilization of the {Re}-^{3}MLCT state. In contrast to mono- and diplatinum cyanido analogs showing appreciable metallophilicity-driven aggregation in solutions, intermolecular association is considerably diminished for bimetallic species **1–4**.

In the solid state, the title compounds are moderately to intensely luminescent with quantum yields substantially exceeding those of the monometallic complexes. The photophysical behavior of solid **1–4** is defined by the platinum(II)-based luminophores, as well as by stimuli-responsive {Pt}···{Pt} interactions, which in turn depend on the bridging ligand and the counteranion. Upon grinding, intense yellow-green {Pt}-based ^{3}(ML/ILCT) luminescence of crystalline complexes **2–4** with quantum yield reaching 0.78 changes to orange-red emissions of amorphous phases. The reverse transition restoring crystallinity can be realized not only by conventional exposure of the samples to solvent vapors, but also by anneal-

 This journal is © the Partner Organisations 2026

Open Access Article. Published on 01 June 2026. Downloaded on 6/3/2026 5:39:24 AM. This article is licensed under a Creative Commons Attribution 3.0 Unported Licence.

ing at moderate temperatures of *ca.* 380 K. This facile thermal crystallization could be ascribed to a soft nature of materials containing bulky borate anions, which allow relatively easy intermolecular rearrangement. In particular, for the bent thiocyanato complexes **4** and **4a**, several distinct structural arrangements with different emission energies were identified. The preferential mode of {Pt}···{Pt} intermolecular stacking is primarily governed by anions. The sterically demanding and hydrophobic fluorinated borate disfavors aggregation *via* metallophilic contacts giving a stable crystalline phase with ^{3}(ML/ILCT) configuration of the excited state, which can be converted mechanically to a metastable amorphous form featuring low-energy ^{3}(MMLCT) phosphorescence. Contrarily, the compact triflate anion stabilizes dimers with metal···metal interactions and red-emitting ^{3}(MMLCT) states, which depend on intermolecular orientation. The latter can be switched between head-to-head and head-to-tail in different solvated forms and by mechanical force probably *via* the rotation around Pt···Pt bond. Albeit the {Re(phen)(CO)$_3$} unit likely remains silent in the solid-state luminescence, together with the SCN$^-$ bridge it plays an important role in guiding intermolecular packing and anchoring variety of aggregation stages in **4** and **4a**.

With these results, we demonstrate that optical and responsive properties of molecular materials based on conventional platinum cyclometalated luminophores can be diversified by realizing hetero-bimetallic systems. In addition to intramolecular structural variations, the anionic counterparts serve as tools for tuning the stability of different {Pt}···{Pt} aggregation modes. The phase transitions related to reorientation of chromophore motifs within noncovalently bound dimers, can be realized in a reversible manner by applying mechanical ↔ vapo/thermal stimuli. The findings provide an understanding of intermolecular relocation as a design principle for programmable solid-state transformations, bridging microscopic dynamics with bulk phase properties.

Author contributions

I. O. K. and C. S. supervised the project and writing – review & editing. I. O. K. and V. V. K. wrote the manuscript. V. V. K. synthesized the compounds, carried out crystallographic and NMR characterization together with A. B. and I. O. K. V. C. performed photophysical studies, with a contribution from A. B. and I. O. K. T. E. and A. J. K. were responsible for computational analysis. All authors participated in the interpretation of the results and the preparation of the final version of the manuscript.

Conflicts of interest

There are no conflicts to declare.

Data availability

The data supporting this article have been included as part of the supplementary information (SI). The original data is available from the authors on request. The authors have cited additional references within the SI.[78–100] Supplementary information: experimental procedures, additional spectroscopic, crystallographic, and computational (XYZ) data. See DOI: https://doi.org/10.1039/d6qi00716c.

CCDC 2541331, 2541332, 2541333, 2541334, 2541335, 2541336, 2541337 and 2554862 contain the supplementary crystallographic data for this paper.[101a–h]

Acknowledgements

We thank the Research Council of Finland (decision 351618, I. O. K.; Flagship Programme, Photonics Research and Innovation PREIN, decision 368653; decision 340584, T. E. and A. J. K.) for financial support. This project has received funding from the European Union – NextGenerationEU instrument and is funded by the Research Council of Finland under grant number 353123. C. A. S. gratefully acknowledges funding from the Deutsche Forschungsgemeinschaft (DFG, German Research Foundation) – FOR 5781: Stimulus-responsive luminescent coordination compounds (STIL-COCOs, project number 535200000), and CRC 1459: Intelligent matter: From responsive to adaptive nanosystems (project number 433682494). Computational resources were provided by the Finnish IT Center for Science (CSC).

References

1 X. Zheng, M. H.-Y. Chan, A. K.-W. Chan, S. Cao, M. Ng, F. K. Sheong, C. Li, E. C. Goonetilleke, W. W. Y. Lam, T.-C. Lau, X. Huang and V. W.-W. Yam, Elucidation of the key role of Pt···Pt interactions in the directional self-assembly of platinum(II) complexes, *Proc. Natl. Acad. Sci.*, 2022, **119**, e2116543119.
2 M. H.-Y. Chan and V. W.-W. Yam, Toward the Design and Construction of Supramolecular Functional Molecular Materials Based on Metal–Metal Interactions, *J. Am. Chem. Soc.*, 2022, **144**, 22805–22825.
3 Y.-C. Wei, K.-H. Kuo, Y. Chi and P.-T. Chou, Efficient Near-Infrared Luminescence of Self-Assembled Platinum(II) Complexes: From Fundamentals to Applications, *Acc. Chem. Res.*, 2023, **56**, 689–699.
4 V. W.-W. Yam and A. S.-Y. Law, Luminescent d^8 metal complexes of platinum(II) and gold(III): From photophysics to photofunctional materials and probes, *Coord. Chem. Rev.*, 2020, **414**, 213298.
5 B. Li, Z. Liang, H. Yan and Y. Li, Visual self-assembly and stimuli-responsive materials based on recent phosphorescent platinum(II) complexes, *Mol. Syst. Des. Eng.*, 2020, **5**, 1578–1605.

Open Access Article. Published on 01 June 2026. Downloaded on 6/3/2026 5:39:24 AM. This article is licensed under a Creative Commons Attribution 3.0 Unported Licence.

6 M. A. Soto, R. Kandel and M. J. MacLachlan, Chromic Platinum Complexes Containing Multidentate Ligands, *Eur. J. Inorg. Chem.*, 2021, **2021**, 894–906.
7 M. Kato, Chromic soft crystals based on luminescent platinum(II) complexes, *IUCrJ*, 2024, **11**, 442–452.
8 M. Han, Y. Tian, Z. Yuan, L. Zhu and B. Ma, A Phosphorescent Molecular "Butterfly" that undergoes a Photoinduced Structural Change allowing Temperature Sensing and White Emission, *Angew. Chem., Int. Ed.*, 2014, **53**, 10908–10912.
9 Z. Shu, Y. Zhang, Z. Ni, G. Xiao, Z. Chi, Y. Li and Y. Ai, Unusual Optical Switches of Platinum(II) Foldamers for Stepwise Photonic Information Storage Materials, *Adv. Opt. Mater.*, 2025, **13**, 2500065.
10 C.-K. Koo, B. Lam, S.-K. Leung, M. H.-W. Lam and W.-Y. Wong, A "Molecular Pivot-Hinge" Based on the pH-Regulated Intramolecular Switching of Pt–Pt and π–π Interactions, *J. Am. Chem. Soc.*, 2006, **128**, 16434–16435.
11 Y. Ai, M. H.-Y. Chan, A. K.-W. Chan, M. Ng, Y. Li and V. W.-W. Yam, A platinum(II) molecular hinge with motions visualized by phosphorescence changes, *Proc. Natl. Acad. Sci. U. S. A.*, 2019, **116**, 13856–13861.
12 M. H.-Y. Chan, S. Y.-L. Leung and V. W.-W. Yam, Rational Design of Multi-Stimuli-Responsive Scaffolds: Synthesis of Luminescent Oligo(ethynylpyridine)-Containing Alkynylplatinum(II) Polypyridine Foldamers Stabilized by Pt···Pt Interactions, *J. Am. Chem. Soc.*, 2019, **141**, 12312–12321.
13 Y. Ai, Y. Zhang, Y. Jiang, G. Zhuang and Y. Li, A stereodynamic probe of Pt(II) molecular h inge for chiroptical sensing of cryptochiral compounds, *Nat. Commun.*, 2025, **16**, 1971.
14 M. Yoshida and M. Kato, Regulation of metal–metal interactions and chromic phenomena of multi-decker platinum complexes having π-systems, *Coord. Chem. Rev.*, 2018, **355**, 101–115.
15 S. J. Choi, J. Kuwabara, Y. Nishimura, T. Arai and T. Kanbara, Two-step Changes in Luminescence Color of Pt(II) Complex Bearing an Amide Moiety by Mechano- and Vapochromism, *Chem. Lett.*, 2011, **41**, 65–67.
16 L. Liu, X. Wang, N. Wang, T. Peng and S. Wang, Bright, Multi-responsive, Sky-Blue Platinum(II) Phosphors Based on a Tetradentate Chelating Framework, *Angew. Chem., Int. Ed.*, 2017, **56**, 9160–9164.
17 C. Cuerva, J. A. Campo, M. Cano and C. Lodeiro, Multi-Stimuli-Responsive Properties of Aggregation-Enhanced Emission-Active Unsymmetrical PtII Metallomesogens through Self-Assembly, *Chem. – Eur. J.*, 2019, **25**, 12046–12051.
18 C.-Y. Lien, Y.-F. Hsu, Y.-H. Liu, S.-M. Peng, T. Shinmyozu and J.-S. Yang, Steric Engineering of Cyclometalated Pt(II) Complexes toward High-Contrast Monomer–Excimer-Based Mechanochromic and Vapochromic Luminescence, *Inorg. Chem.*, 2020, **59**, 11584–11594.
19 Y. Ai, Y. Li, M. H.-Y. Chan, G. Xiao, B. Zou and V. W.-W. Yam, Realization of Distinct Mechano- and Piezochromic Behaviors via Alkoxy Chain Length-Modulated Phosphorescent Properties and Multidimensional Self-Assembly Structures of Dinuclear Platinum(II) Complexes, *J. Am. Chem. Soc.*, 2021, **143**, 10659–10667.
20 D. Gómez de Segura, E. Lalinde and M. T. Moreno, Polymorphism and Mechanochromism in 2-Phenylbenzothiazole Cyclometalated Pt^{II} Complexes with Chelating N^O Ligands, *Inorg. Chem.*, 2022, **61**, 20043–20056.
21 Y. Zhang, J. Ni, Y. Zhu, Q. Zeng, Y. Ai and Y. Li, Multi-stimuli responsive Pt(II) complexes for information storage and anti-counterfeiting, *Chem. Eng. J.*, 2024, **498**, 155049.
22 B.-C. Tzeng, Y.-T. Wu, B.-J. Sun, A. H. H. Chang and S.-Y. Chien, Mechanochromic and Solvent-Induced Luminescence of a Supramolecular Pt(II)-Bipyridine Complex with Di(4-pyridylmethyl)aminedithiocarbamate, *Inorg. Chem.*, 2024, **63**, 18589–18595.
23 Y.-F. Hsu, Y.-C. Ho, Y.-H. Liu and J.-S. Yang, Dual-Phase Multi-Stimuli-Responsive Luminescence from a Pentiptycene-Linked Binuclear Cyclometalated Platinum (II) Complex, *Inorg. Chem.*, 2025, **64**, 16527–16536.
24 X. Du, X. Liu, Q. Liu, L. Zong, X. Xing, X. Cheng, D. Qiu and M.-S. Yuan, Modulating supramolecular Pt···Pt interactions and π–π stacking for high-contrast mechanochromic and vapochromic materials, *Chem. Commun.*, 2025, **61**, 14657–14660.
25 Y. Ai, H. Zhang, Y. Jiang, Y. Zhang, H. Mo, Y. Liu, T. Han, G. Xiao, B. Zou, M. Li, Z. Chi, Y.-W. Zhong and Y. Li, Pressure-Gated Inverse Steric Enforcement in Coordinated Rotors as Programmable Optical Switching for Hierarchical Information Encryption, *Adv. Opt. Mater.*, 2026, **14**, e03017.
26 M. Yoshida and M. Kato, Cation-controlled luminescence behavior of anionic cyclometalated platinum(II) complexes, *Coord. Chem. Rev.*, 2020, **408**, 213194.
27 M. Yoshida and M. Kato, Control of Pt···Pt interactions in Pt(II) complex crystals as luminescence sensors for the detection of external stimuli: recent achievements and perspectives, *Anal. Sci.*, 2025, **41**, 1233–1249.
28 Y. Ma, K. Chen, J. Lu, J. Shen, C. Ma, S. Liu, Q. Zhao and W.-Y. Wong, Phosphorescent Soft Salt Based on Platinum (II) Complexes: Photophysics, Self-Assembly, Thermochromism, and Anti-counterfeiting Application, *Inorg. Chem.*, 2021, **60**, 7510–7518.
29 J. Li, K. Chen, J. Wei, Y. Ma, R. Zhou, S. Liu, Q. Zhao and W.-Y. Wong, Reversible On–Off Switching of Excitation-Wavelength-Dependent Emission of a Phosphorescent Soft Salt Based on Platinum(II) Complexes, *J. Am. Chem. Soc.*, 2021, **143**, 18317–18324.
30 X. Lei, Y. Ai, Z. Shu, W. Wang and Y. Li, Precise Regulation the Multiemission Based on Soft Double Salt for Information Encryption, *Inorg. Chem.*, 2024, **63**, 11354–11360.
31 A. Rico, P. Le Poul, J. Rodríguez-López, S. Achelle and S. Gauthier, Exploring structural and optical properties of

 This journal is © the Partner Organisations 2026

Open Access Article. Published on 01 June 2026. Downloaded on 6/3/2026 5:39:24 AM. This article is licensed under a Creative Commons Attribution 3.0 Unported Licence.

a new series of soft salts based on cyclometalated platinum complexes, *Dalton Trans.*, 2024, **53**, 11417–11425.

32 A. Rico, P. Le Poul, A. Lyčka, J. Rodríguez-López, S. Achelle and S. Gauthier, Cyclometalated platinum(II) complex-based soft salt with multistimuli-responsive properties, *New J. Chem.*, 2025, **49**, 8494–8501.

33 A. Rico, P. Le Poul, J. Rodríguez-López, D. Jacquemin, S. Achelle and S. Gauthier, Multistimuli-Responsive Chromic Properties of Soft Salts Based on Cyclometalated Platinum(II) Complexes: Pyridine- vs. Pyrimidine-Based Ligands, *ChemPhotoChem*, 2025, **9**, e202500164.

34 M. J. Bryant, J. M. Skelton, L. E. Hatcher, C. Stubbs, E. Madrid, A. R. Pallipurath, L. H. Thomas, C. H. Woodall, J. Christensen, S. Fuertes, T. P. Robinson, C. M. Beavers, S. J. Teat, M. R. Warren, F. Pradaux-Caggiano, A. Walsh, F. Marken, D. R. Carbery, S. C. Parker, N. B. McKeown, R. Malpass-Evans, M. Carta and P. R. Raithby, A rapidly-reversible absorptive and emissive vapochromic Pt(II) pincer-based chemical sensor, *Nat. Commun.*, 2017, **8**, 1800.

35 M. Martínez-Junquera, E. Lalinde and M. T. Moreno, Multistimuli-Responsive Properties of Aggregated Isocyanide Cycloplatinated(II) Complexes, *Inorg. Chem.*, 2022, **61**, 10898–10914.

36 D. Saito, T. Galica, E. Nishibori, M. Yoshida, A. Kobayashi and M. Kato, Reversible and Stepwise Single-Crystal-to-Single-Crystal Transformation of a Platinum(II) Complex with Vapochromic Luminescence, *Chem. – Eur. J.*, 2022, **28**, e202200703.

37 C. L. Stubbs, M. J. Bryant, L. E. Hatcher and P. R. Raithby, Manipulating vapochromic or solvatochromic properties of platinum(II) pincer complexes through ligand modifications, *CrystEngComm*, 2025, **27**, 7498–7513.

38 J.-C. Chen, Z.-L. Gong, Z.-Q. Li, Y.-Y. Zhao, K. Tang, D.-X. Ma, F.-F. Xu and Y.-W. Zhong, Vaporchromic Domino Transformation and Polarized Photonic Heterojunctions of Organoplatinum Microrods, *Angew. Chem., Int. Ed.*, 2024, **63**, e202412651.

39 J. Quan, Z.-H. Chen, X. Zhang, J.-Y. Wang, L.-Y. Zhang and Z.-N. Chen, Geometrically isomeric Pt_2Ag_2 acetylide complexes of 2,6-bis(diphenylphosphino)pyridine: luminescent and vapochromic properties, *Inorg. Chem. Front.*, 2021, **8**, 2323–2332.

40 M. Sadeghian, D. Gómez de Segura, M. Golbon Haghighi, N. Safari, E. Lalinde and M. T. Moreno, Ladder-like heteropolynuclear assemblies via cyanido bridges and platinum(II)–thallium(I) bonds: structural and photophysical properties, *Dalton Trans.*, 2024, **53**, 7788–7800.

41 X.-N. Hu, X.-H. Zhong, R.-R. Zhong, L.-M. Zhang, D.-B. Hao, Q. Xu, H.-Z. Wei, R. Zhou, J. Wei, K.-G. Liu, S.-F. Yuan, D.-S. Li and T. Wu, Significantly enhanced NIR emission of solid-state clusters based on Cu_4Pt_2 triggered with volatile organic compounds, *Nanoscale*, 2025, **17**, 5829–5837.

42 B. Ventura, A. Barbieri, F. Barigelletti, S. Diring and R. Ziessel, Energy Transfer Dynamics in Multichromophoric Arrays Engineered from Phosphorescent PtII/RuII/OsII Centers Linked to a Central Truxene Platform, *Inorg. Chem.*, 2010, **49**, 8333–8346.

43 V. H. Nguyen, B. Kandasamy and J. H. K. Yip, Coupling d^6 Ir(III) and d^8 Pt(II) Chromophores, *Inorg. Chem.*, 2018, **57**, 4699–4718.

44 Y.-S. Wong, M. Ng, M. C.-L. Yeung and V. W.-W. Yam, Platinum(II)-Based Host–Guest Coordination-Driven Supramolecular Co-Assembly Assisted by Pt···Pt and π–π Stacking Interactions: A Dual-Selective Luminescence Sensor for Cations and Anions, *J. Am. Chem. Soc.*, 2021, **143**, 973–982.

45 P. A. Smith, C. Crawford, N. Beedoe, Z. Assefa and R. E. Sykora, Synthesis, Crystal Structures, and Dual Donor Luminescence Sensitization in Novel Terbium Tetracyanoplatinates, *Inorg. Chem.*, 2012, **51**, 12230–12241.

46 K. S. Kisel, A. S. Melnikov, E. V. Grachova, A. J. Karttunen, A. Doménech-Carbó, K. Y. Monakhov, V. G. Semenov, S. P. Tunik and I. O. Koshevoy, Supramolecular construction of cyanide-bridged Re^I diimine multichromophores, *Inorg. Chem.*, 2019, **58**, 1988–2000.

47 M. El Sayed Moussa, A. M. Khalil, S. Evariste, H.-L. Wong, V. Delmas, B. Le Guennic, G. Calvez, K. Costuas, V. W.-W. Yam and C. Lescop, Intramolecular rearrangements guided by adaptive coordination-driven reactions toward highly luminescent polynuclear Cu(i) assemblies, *Inorg. Chem. Front.*, 2020, **7**, 1334–1344.

48 A. S. Sergeenko, D. Paripovic, C. Dab, P.-F. Blanc, C. Reber and D. B. Leznoff, Highly emissive polymorphs of anhydrous cadmium tetracyanoplatinate and their solvated coordination networks, *Dalton Trans.*, 2022, **51**, 9531–9540.

49 L. M. Karn, A. Britton and D. B. Leznoff, Inducing Platinophilic Interactions in $[Pt(SCN)_4]^{2-}$ Salts by Cation Tuning, *Inorg. Chem.*, 2024, **63**, 11977–11985.

50 M. Wyczesany, M. Heczko, M. Reczyński, B. Sieklucka and S. Chorazy, Optical memory effect in a dynamic gadolinium–tetracyanidoplatinate coordination polymer for sensing deviations in temperature and humidity, *J. Mater. Chem. C*, 2025, **13**, 2732–2744.

51 A. Kobayashi, Y. Fukuzawa, H.-C. Chang and M. Kato, Vapor-Controlled Linkage Isomerization of a Vapochromic Bis(thiocyanato)platinum(II) Complex: New External Stimuli To Control Isomerization Behavior, *Inorg. Chem.*, 2012, **51**, 7508–7519.

52 C. Wakasugi, M. Yoshida, W. M. C. Sameera, Y. Shigeta, A. Kobayashi and M. Kato, Bright Luminescent Platinum (II)-Biaryl Emitters Synthesized Without Air-Sensitive Reagents, *Chem. – Eur. J.*, 2020, **26**, 5449–5458.

53 T.-O. Knedel, S. Buss, I. Maisuls, C. G. Daniliuc, C. Schlüsener, P. Brandt, O. Weingart, A. Vollrath, C. Janiak and C. A. Strassert, Encapsulation of Phosphorescent Pt(II) Complexes in Zn-Based Metal–Organic Frameworks toward Oxygen-Sensing Porous Materials, *Inorg. Chem.*, 2020, **59**, 7252–7264.

Open Access Article. Published on 01 June 2026. Downloaded on 6/3/2026 5:39:24 AM. This article is licensed under a Creative Commons Attribution 3.0 Unported Licence.

54 R. J. Salthouse, P. Pander, D. S. Yufit, F. B. Dias and J. A. G. Williams, Near-infrared electroluminescence beyond 940 nm in Pt(N^C^N)X complexes: influencing aggregation with the ancillary ligand X, *Chem. Sci.*, 2022, **13**, 13600–13610.

55 K. Sasaki, D. Saito, M. Yoshida, F. Tanaka, A. Kobayashi, K. Sada and M. Kato, Chromic triboluminescence of self-assembled platinum(II) complexes, *Chem. Commun.*, 2023, **59**, 6745–6748.

56 M. Sadeghian, D. Gómez de Segura, M. G. Haghighi, N. Safari, E. Lalinde and M. T. Moreno, Luminescent Anionic Cyclometalated Organoplatinum(II) Complexes with Terminal and Bridging Cyanide Ligand: Structural and Photophysical Properties, *Inorg. Chem.*, 2023, **62**, 1513–1529.

57 V. V. Khistiaeva, S. Buss, T. Eskelinen, P. Hirva, N. Kinnunen, J. Friedel, L. Kletsch, A. Klein, C. A. Strassert and I. O. Koshevoy, Cyanido-bridged diplatinum(II) complexes: ligand and solvent effect on aggregation and luminescence, *Chem. Sci.*, 2024, **15**, 4005–4018.

58 V. Sivchik, A. Kochetov, T. Eskelinen, K. S. Kisel, A. I. Solomatina, E. V. Grachova, S. P. Tunik, P. Hirva and I. O. Koshevoy, Modulation of Metallophilic and π–π Interactions in Platinum Cyclometalated Luminophores with Halogen Bonding, *Chem. – Eur. J.*, 2021, **27**, 1787–1794.

59 S. M. Fredericks, J. C. Luong and M. S. Wrighton, Multiple Emissions from Rhenium(I) Complexes: Intraligand and Charge-Transfer Emission from Substituted Metal Carbonyl Cations, *J. Am. Chem. Soc.*, 1979, **101**, 7415–7417.

60 W.-K. Chu, X.-G. Wei, S.-M. Yiu, C.-C. Ko and K.-C. Lau, Strongly Phosphorescent Neutral Rhenium(I) Isocyanoborato Complexes: Synthesis, Characterization, and Photophysical, Electrochemical, and Computational Studies, *Chem. – Eur. J.*, 2015, **21**, 2603–2612.

61 Y. Xiao, A. W.-Y. Cheung, S.-W. Lai, S.-C. Cheng, S.-M. Yiu, C.-F. Leung and C.-C. Ko, Electronic Communication in Luminescent Dicyanorhenate-Bridged Homotrinuclear Rhenium(I) Complexes, *Inorg. Chem.*, 2019, **58**, 6696–6705.

62 L. Schneider, V. Sivchik, K.-y. Chung, Y.-T. Chen, A. J. Karttunen, P.-T. Chou and I. O. Koshevoy, Cyclometalated Platinum(II) Cyanometallates: Luminescent Blocks for Coordination Self-Assembly, *Inorg. Chem.*, 2017, **56**, 4459–4467.

63 E. Rossi, A. Colombo, C. Dragonetti, D. Roberto, F. Demartin, M. Cocchi, P. Brulatti, V. Fattori and J. A. G. Williams, From red to near infra-red OLEDs: the remarkable effect of changing from X = –Cl to –NCS in a cyclometallated [Pt(N^C^N)X] complex {N^C^N = 5-mesityl-1,3-di-(2-pyridyl)benzene}, *Chem. Commun.*, 2012, **48**, 3182–3184.

64 M. Wrighton and D. L. Morse, Nature of the Lowest Excited State in Tricarbonylchloro-1,10-phenanthrolinerhenium(I) and Related Complexes, *J. Am. Chem. Soc.*, 1974, **96**, 998–1003.

65 L. Wallace and D. P. Rillema, Photophysical Properties of Rhenium(I) Tricarbonyl Complexes Containing Alkyl- and Aryl-Substituted Phenanthrolines as Ligands, *Inorg. Chem.*, 1993, **32**, 3836–3843.

66 K. S. Kisel, A. S. Melnikov, E. V. Grachova, P. Hirva, S. P. Tunik and I. O. Koshevoy, Linking Re(I) and Pt(II) chromophores with aminopyridines: a simple route to achieve a complicated photophysical behavior, *Chem. – Eur. J.*, 2017, **23**, 11301–11311.

67 T. Eskelinen, S. Buss, S. K. Petrovskii, E. V. Grachova, M. Krause, L. Kletsch, A. Klein, C. A. Strassert, I. O. Koshevoy and P. Hirva, Photophysics and Excited State Dynamics of Cyclometalated [M(Phbpy)(CN)] (M = Ni, Pd, Pt) Complexes: A Theoretical and Experimental Study, *Inorg. Chem.*, 2021, **60**, 8777–8789.

68 J. E. Yarnell, J. C. Deaton, C. E. McCusker and F. N. Castellano, Bidirectional "Ping-Pong" Energy Transfer and 3000-Fold Lifetime Enhancement in a Re(I) Charge Transfer Complex, *Inorg. Chem.*, 2011, **50**, 7820–7830.

69 Z. Jin, S. Qi, X. Guo, N. Tian, Y. Hou, C. Li, X. Wang and Q. Zhou, Smart use of "ping-pong" energy transfer to improve the two-photon photodynamic activity of an Ir(iii) complex, *Chem. Commun.*, 2020, **56**, 2845–2848.

70 Q. Zheng, S. Borsley, T. Tu and S. L. Cockroft, Reversible stimuli-responsive chromism of a cyclometallated platinum(II) complex, *Chem. Commun.*, 2020, **56**, 14705–14708.

71 W. Lu, Y. Chen, V. A. L. Roy, S. S.-Y. Chui and C.-M. Che, Supramolecular Polymers and Chromonic Mesophases Self-Organized from Phosphorescent Cationic Organoplatinum(II) Complexes in Water, *Angew. Chem., Int. Ed.*, 2009, **48**, 7621–7625.

72 X.-P. Zhang, J.-F. Mei, J.-C. Lai, C.-H. Li and X.-Z. You, Mechano-induced luminescent and chiroptical switching in chiral cyclometalated platinum(II) complexes, *J. Mater. Chem. C*, 2015, **3**, 2350–2357.

73 Y. Shigeta, T. Nomoto, M. Kato and M. Mizuno, Mechanical and Thermal ON–OFF Switching of the Vapochromic Behavior of a Luminescent Polymorphic Pt (II) Complex, *Inorg. Chem.*, 2023, **62**, 66–74.

74 X.-T. Lv, D. Zheng, F.-S. Wan, Y.-L. Liu, Z.-H. Guo, D.-K. Cao and X.-L. Yang, Pt(II) Complexes Showing Multicolor Emissions from Nanoparticles in Solution and Reversible Grinding- and Heating-Induced Luminescence Switching in Solid State, *Chem. – Eur. J.*, 2025, **31**, e202403886.

75 Y. Shigeta, A. Kobayashi, M. Yoshida and M. Kato, Crystal Engineering of Vapochromic Porous Crystals Composed of Pt(II)-Diimine Luminophores for Vapor-History Sensors, *Cryst. Growth Des.*, 2018, **18**, 3419–3427.

76 V. W.-W. Yam, K. H.-Y. Chan, K. M.-C. Wong and N. Zhu, Luminescent Platinum(II) Terpyridyl Complexes: Effect of Counter Ions on Solvent-Induced Aggregation and Color Changes, *Chem. – Eur. J.*, 2005, **11**, 4535–4543.

77 A. Paderina, S. Slavova, E. Tupikina, D. Snetkov and E. Grachova, Aggregation Game: Changing Solid-State

 This journal is © the Partner Organisations 2026

Open Access Article. Published on 01 June 2026. Downloaded on 6/3/2026 5:39:24 AM. This article is licensed under a Creative Commons Attribution 3.0 Unported Licence.

Emission Using Different Counterions in Monoalkynylphosphonium Pt(II) Complexes, *Inorg. Chem.*, 2024, **63**, 17548–17560.

78 P. Kurz, B. Probst, B. Spingler and R. Alberto, Ligand Variations in [ReX(diimine)$(CO)_3$] Complexes: Effects on Photocatalytic CO_2 Reduction, *Eur. J. Inorg. Chem.*, 2006, **2006**, 2966–2974.

79 V. V. Sivchik, E. V. Grachova, A. S. Melnikov, S. N. Smirnov, A. Y. Ivanov, P. Hirva, S. P. Tunik and I. O. Koshevoy, Solid state and solution metallophilic aggregation of a cationic $[Pt(NCN)]^+$ cyclometalated complex, *Inorg. Chem.*, 2016, **55**, 3351–3363.

80 M. Mosberger, B. Probst, B. Spingler and R. Alberto, Influence of Hetero-Biaryl Ligands on the Photo-Electrochemical Properties of $[Re^{I}NCS(N^{\cap}N)(CO)_3]$-Type Photosensitizers, *Eur. J. Inorg. Chem.*, 2019, **2019**, 3518–3525.

81 *APEX2 – Software Suite for Crystallographic Programs*, Bruker AXS, Inc., 2010.

82 *CrysAlisPro, Rigaku Oxford Diffraction, 1.171.43.144a*, 2024.

83 G. M. Sheldrick, *SADABS-2008/1 – Bruker AXS Area Detector Scaling and Absorption Correction*, Bruker AXS, 2008.

84 G. M. Sheldrick, Crystal structure refinement with SHELXL, *Acta Crystallogr., Sect. C: Struct. Chem.*, 2015, **71**, 3–8.

85 L. J. Farrugia, WinGX and ORTEP for Windows: an Update, *J. Appl. Crystallogr.*, 2012, **45**, 849–854.

86 O. V. Dolomanov, L. J. Bourhis, R. J. Gildea, J. A. K. Howard and H. Puschmann, OLEX2: A complete structure solution, refinement and analysis program, *J. Appl. Crystallogr.*, 2009, **42**, 339–341.

87 A. L. Spek, PLATON SQUEEZE: a tool for the calculation of the disordered solvent contribution to the calculated structure factors, *Acta Crystallogr., Sect. C:Struct. Chem.*, 2015, **71**, 9–18.

88 A. Sillen and Y. Engelborghs, The Correct Use of "Average" Fluorescence Parameters, *Photochem. Photobiol.*, 1998, **67**, 475–486.

89 F. Neese, Software update: The ORCA program system - Version 5.0, *Wiley Interdiscip. Rev.: Comput. Mol. Sci.*, 2022, e1606.

90 F. Weigend and R. Ahlrichs, Balanced Basis Sets of Split Valence, Triple Zeta Valence and Quadruple Zeta Valence Quality for H to Rn: Design and Assessment of Accuracy, *Phys. Chem. Chem. Phys.*, 2005, **7**, 3297–3305.

91 E. v. Lenthe, E. J. Baerends and J. G. Snijders, Relativistic regular two–component Hamiltonians, *J. Chem. Phys.*, 1993, **99**, 4597–4610.

92 C. van Wüllen, Molecular density functional calculations in the regular relativistic approximation: Method, application to coinage metal diatomics, hydrides, fluorides and chlorides, and comparison with first-order relativistic calculations, *J. Chem. Phys.*, 1998, **109**, 392–399.

93 B. de Souza, G. Farias, F. Neese and R. Izsák, Predicting Phosphorescence Rates of Light Organic Molecules Using Time-Dependent Density Functional Theory and the Path Integral Approach to Dynamics, *J. Chem. Theory Comput.*, 2019, **15**, 1896–1904.

94 J. D. Rolfes, F. Neese and D. A. Pantazis, All-electron scalar relativistic basis sets for the elements Rb–Xe, *J. Comput. Chem.*, 2020, **41**, 1842–1849.

95 M. A. Rohrdanz, K. M. Martins and J. M. Herbert, A long-range-corrected density functional that performs well for both ground-state properties and time-dependent density functional theory excitation energies, including charge-transfer excited states, *J. Chem. Phys.*, 2009, **130**, 054112.

96 J. P. Perdew, K. Burke and M. Ernzerhof, Generalized Gradient Approximation Made Simple, *Phys. Rev. Lett.*, 1996, **77**, 3865–3868.

97 C. Adamo and V. Barone, Toward reliable density functional methods without adjustable parameters: The PBE0 model, *J. Chem. Phys.*, 1999, **110**, 6158–6170.

98 V. Barone and M. Cossi, Quantum Calculation of Molecular Energies and Energy Gradients in Solution by a Conductor Solvent Model, *J. Phys. Chem. A*, 1998, **102**, 1995–2001.

99 F. Neese, An improvement of the resolution of the identity approximation for the formation of the Coulomb matrix, *J. Comput. Chem.*, 2003, **24**, 1740–1747.

100 F. Neese, F. Wennmohs, A. Hansen and U. Becker, Efficient, approximate and parallel Hartree–Fock and hybrid DFT calculations. A 'chain-of-spheres' algorithm for the Hartree–Fock exchange, *Chem. Phys.*, 2009, **356**, 98–109.

101 (*a*) CCDC 2541331: Experimental Crystal Structure Determination, 2026, DOI: **10.5517/ccdc.csd.cc2r9gfz**; (*b*) CCDC 2541332: Experimental Crystal Structure Determination, 2026, DOI: **10.5517/ccdc.csd.cc2r9gg0**; (*c*) CCDC 2541333: Experimental Crystal Structure Determination, 2026, DOI: **10.5517/ccdc.csd.cc2r9gh1**; (*d*) CCDC 2541334: Experimental Crystal Structure Determination, 2026, DOI: **10.5517/ccdc.csd.cc2r9gj2**; (*e*) CCDC 2541335: Experimental Crystal Structure Determination, 2026, DOI: **10.5517/ccdc.csd.cc2r9gk3**; (*f*) CCDC 2541336: Experimental Crystal Structure Determination, 2026, DOI: **10.5517/ccdc.csd.cc2r9gl4**; (*g*) CCDC 2541337: Experimental Crystal Structure Determination, 2026, DOI: **10.5517/ccdc.csd.cc2r9gm5**; (*h*) CCDC 2554862: Experimental Crystal Structure Determination, 2026, DOI: **10.5517/ccdc.csd.cc2rrjxz**.